Gain-Induced Trapping of Microcavity Exciton Polariton Condensates

Georgios Roumpos,[1,*] Wolfgang H. Nitsche,[1] Sven Höfling,[2] Alfred Forchel,[2] and Yoshihisa Yamamoto[1,3]

[1]*E. L. Ginzton Laboratory, Stanford University, Stanford, California, 94305, USA*

[2]*Technische Physik, University of Würzburg Wilhelm-Conrad-Röntgen-Research Center for Complex Material Systems, Germany*

[3]*National Institute of Informatics, Hitotsubashi, Chiyoda-ku, Tokyo 101-8430, Japan*

(Received 2 December 2009; published 26 March 2010)

We have performed real and momentum space spectroscopy of exciton polariton condensates in a GaAs-based microcavity under nonresonant excitation with an intensity-stabilized laser. An effective trapping mechanism is revealed, which is due to the stimulated scattering gain inside the finite excitation spot combined with the short lifetime. We observe several quantized modes while the lowest state shows Heisenberg-limited real and momentum space distributions. The experimental findings are qualitatively reproduced by an open dissipative Gross-Pitaevskii equation model.

DOI: 10.1103/PhysRevLett.104.126403 PACS numbers: 71.36.+c, 03.75.Nt, 78.67.De, 78.70.−g

It is well known that an infinite two-dimensional (2D) system cannot establish true long-range order above zero temperature because of phase fluctuations [1,2]. But when a trapping mechanism is employed, so that the system size is finite, a crossover temperature exists below which there are sizable correlations across the trap. For example, a 2D system of ideal bosons in a trap is expected to show Bose Einstein condensation below a temperature that depends on the trap size and shape [3].

Microcavity exciton polaritons [4] is a 2D system that behaves as bosonic at low densities. Although the particle lifetime is short, limited by the photon lifetime inside the cavity, so that true thermal equilibrium cannot be established, a dynamical condensation phenomenon similar to Bose Einstein condensation is observed [5,6]. Free electron-hole pairs are optically injected, which then relax towards the lower polariton branch. Above a threshold laser pumping power the scattering rate towards one or a few final states is significantly enhanced due to the bosonic final state stimulation, and condensation occurs. It has been proposed that external trapping such as photonic disorder [7], stress trap [8], micropillar patterning [9], or metal film [10] is essential to stabilize a spatial mode.

Here, we show that there is an implicit confinement mechanism due to the finite lifetime and the spacially confined gain inside the finite excitation spot size. Namely, reservoir polaritons cannot travel far from the point where they were created and final state stimulation only occurs inside the laser excitation spot area where polariton density is sufficient. Under suitable excitation conditions, we can observe the quantized states of this effective trap in real as well as in momentum space. Only the lowest state is perturbed by the disorder potential and it is further confined by the latter. We have observed Heisenberg-limited real and momentum space distributions for this state, which confirms that phase fluctuations are negligible. We use a simplified one-dimensional model, employing a generalized Gross-Pitaevskii equation with loss and gain terms, to qualitatively reproduce our experimental results.

The sample is the same as in our recent experiments [11,12], and it consists of an AlAs $\frac{\lambda}{2}$ cavity sandwiched between two distributed Bragg reflector mirrors. The upper and lower mirrors are made of 16 and 20 pairs, respectively, of AlAs and $Ga_{0.8}Al_{0.2}As$. Three stacks of 4 GaAs quantum wells are grown at the central three antinodes of the cavity. The measurements reported here are taken from a spot on the sample with photon-exciton detuning $\delta = -2$ meV, while the Rabi splitting is $2\hbar\Omega_{\mathrm{Rabi}} = 14$ meV. The sample is kept at a temperature of 7–8 K on the cold finger of a He flow cryostat. The system is pumped with a single-frequency Ti-Sapphire ring laser focused on a flat spot of diameter ~ 25 μm (as measured for low pumping power) from the direction normal to the sample [12]. The laser is linearly polarized, and the orthogonal linear polarization is detected. Luminescence above threshold is almost unpolarized, namely, the degree of linear polarization is <0.15. This is attributed to the small ground state linear polarization splitting, typically ~ 50 μeV in our sample [11]. We expect that the condensate randomly chooses one direction of linear polarization in every realization; therefore, luminescence appears almost unpolarized after time-averaged detection. The laser wavelength is tuned to the first reflectivity minimum of the cavity above the stop band and it is modulated into pulses with 0.5 ms duration and 100 Hz repetition rate to prevent sample heating. Luminescence is collected through an objective lens with numerical aperture NA = 0.55. The spectroscopy setup is the same as in [11] and allows us to perform near field (NF—real space) and far field (FF—momentum space) imaging and spectroscopy. That is, we can measure energy-resolved luminescence as a function of position or of in-plane momentum. Our resolution is 1 μm for NF spectroscopy and 0.05 $\mu\mathrm{m}^{-1}$ for FF spectroscopy.

Above a threshold pumping power of 70 mW, the phase transition from normal to condensation states is observed

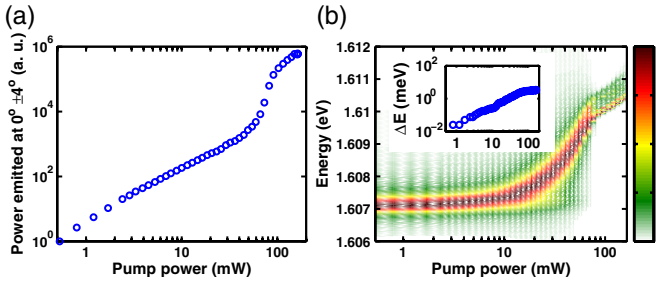

FIG. 1 (color online). Evidence for polariton condensation. (a) Power emitted between ±4° as a function of pumping power. A nonlinear increase is evident at a threshold power of 70 mW. (b) Normalized spectra as a function of power. Above threshold, several narrow peaks appear. Inset: Energy shift of the main spectral peak as a function of power. The linear blue shift below threshold is followed by a logarithmic shift above threshold.

(Fig. 1): the power emitted at small angles increases nonlinearly, spectral peaks with reduced linewidth appear and the energy blue shift changes from a linear dependence on the pumping power to a logarithmic dependence [9]. Figure 2 shows real space and momentum space spectra measured above threshold. Six discrete modes appear whose linewidth is resolution limited. Our spectral resolution has HWHM ~ 25 μeV, corresponding to coherence time $\hbar/\mathrm{HWHM} = 26$ ps.

In order to move the real or momentum space image along one direction, we move the last lens of our optical system (the one in front of the spectrometer) along the same direction perpendicular to the optical axis. The translation is also perpendicular to the direction of the spectrometer slit. This way, we can record spectra along parallel lines in real or momentum space resulting in a 2D grid of spectrally-resolved luminescence. We can then integrate around the energy of each mode and generate 2D images of the different modes in real [Fig. 3(a)] as well as in momentum [Fig. 4(a)–4(f)] space.

Inside a circular trap with infinite barrier height, the solutions of the Schrödinger equation are expressed in terms of Bessel functions of the first kind

$$\psi_{mn}(r, \phi) \propto e^{im\phi} J_m(k_n r), \qquad k_n = \frac{j_{mn}}{R_0}, \qquad (1)$$

where R_0 is the trap radius and j_{mn} are the roots of the Bessel function $J_m(x)$ for $n = 1, 2, 3, \ldots$. The FF wave functions follow from the Fourier transform of the above expression. Based on this, we can assign quantum numbers (m, n) to the six observed modes as shown in Figs. 3 and 4.

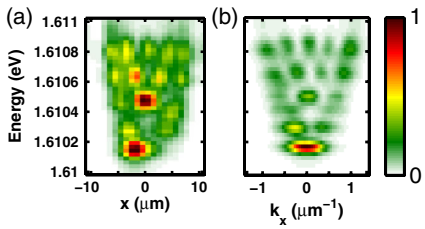

FIG. 2 (color online). (a) Real space and (b) momentum space spectra measured above threshold (at 115 mW).

The real space images show the characteristics of the above wave functions. The comparison is shown in Fig. 3(b)–3(g) for a trap of radius 8 μm. This radius is shorter than the spot radius measured below threshold ($\sim$12.5 μm), as the spot shrinks above threshold. This is because the lifetime of the excitations we create drops from $\sim$200 ps below threshold to a few ps above threshold, as measured for our sample and excitation conditions, so that they do not have enough time to diffuse. This is due to the bosonic final state stimulation effect, namely, the relaxation rate is proportional to the population of the final state, so it is accelerated above the condensation threshold [13]. For example, a polariton of mass $6 \times 10^{-5} m_e$ and momentum $k_x = 0.5$ μm^{-1} can only move by 2 μm in 2 ps. The inability of polaritons to escape from the pumping spot creates a finite-size gain region that traps condensates inside it. This is a similar mechanism to gain guiding in semiconductor laser structures [14].

The same model works for the momentum space images, as shown in Figs. 4(g)–4(l). We note that the harmonic potential model could not explain the energy splitting between modes (2, 1) and (0, 2) (3rd and 4th modes), which is clear in Fig. 2(b). Also, the modes $(m, n) =$ (3, 1), (4, 1), (2, 2), which should appear among the observed modes, are missing since their large angular momentum makes polariton scattering into these states inefficient.

The sample disorder potential follows a Gaussian distribution with standard deviation $<$0.1 meV [12], which is

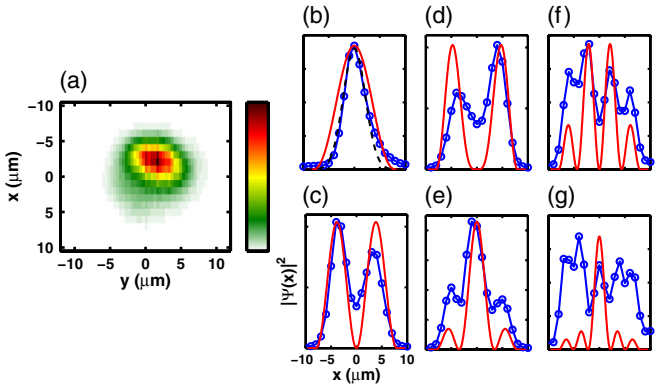

FIG. 3 (color online). (a) Experimental 2D real space image of the lowest trapped state with quantum numbers $(m, n) = (0, 1)$. (b–g) 1D mode profiles. Blue (dark in print): experiment, red (gray in print): trapped states of an infinite circular quantum well of radius 8 μm. In (b) we have integrated along the y axis, and also fitted the experimental profile with a Gaussian distribution (black dashed line). (c–g) are simple cross sections along the x axis at $y = 0$ μm. The quantum numbers (m, n) are (b) (0, 1), (c) (1, 1), (d) (2, 1), (e) (0, 2), (f) (1, 2), and (g) (0, 3).

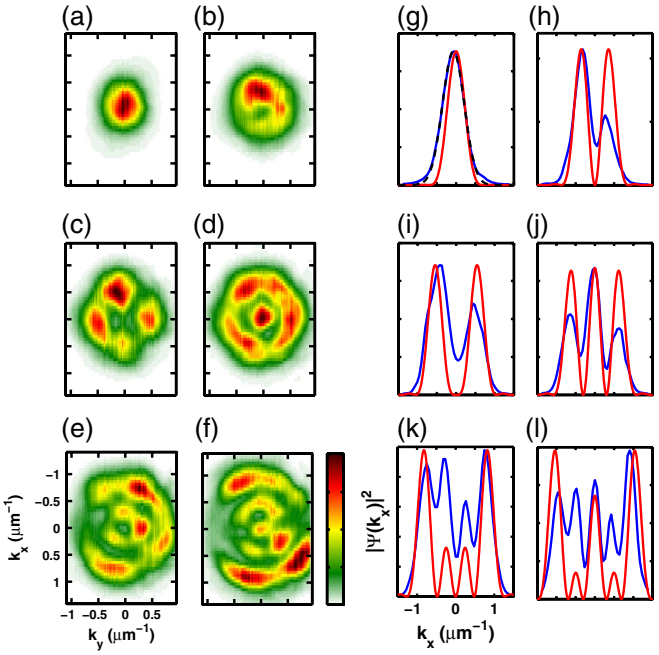

FIG. 4 (color online). (a–f) Experimental 2D momentum space images of trapped states. The quantum numbers (m, n) are (a) (0, 1), (b) (1, 1), (c) (2, 1), (d) (0, 2), (e) (1, 2), and (f) (0, 3). (g–l) 1D mode profiles. Blue (dark in print): experiment, red (gray in print): trapped states of an infinite circular quantum well of radius 8 μm. In (g) we have integrated along the k_y axis, and also fitted the experimental profile with a Gaussian distribution (black dashed line). (h–l) are simple cross sections along $k_y = 0\ \mu\text{m}^{-1}$. The quantum numbers (m, n) are (g) (0, 1), (h) (1, 1), (i) (2, 1), (j) (0, 2), (k) (1, 2), and (l) (0, 3).

considerably smaller than the kinetic energy of all modes except the lowest one, as shown on the measured spectra of Fig. 2. Indeed, only the lowest mode is perturbed by the disorder potential and it is further confined. Figure 3(a) shows that the lowest mode has migrated away from the center of the beam, possibly towards a local minimum of the disorder potential. In Fig. 3(b) we plot the measured profile of this mode along the x axis, where we have integrated Fig. 3(a) along the y axis and shifted the result to center it around $x = 0\ \mu$m (instead, Figs. 3(c)–3(g) are simple cross sections along $y = 0\ \mu$m). The observed distribution is narrower than the expected one based on the infinite quantum well model. We can fit it with a Gaussian (dashed line) with standard deviation $\sigma_x = 2.16\ \mu$m. The same effect is evident in the momentum space distribution of the lowest mode [Fig. 4(g)], which is wider than the model prediction. Fitting with a Gaussian gives a standard deviation of $\sigma_{k_x} = 0.283\ \mu\text{m}^{-1}$. Taking the product $\sigma_x \times \sigma_{k_x} = 0.61$, which is very close to the Heisenberg limit of 0.5.

The stabilized intensity of the excitation laser is critical for our observations. In [12], we used a mode-locked Ti-Sapphire laser operated in the continuous wave mode. As the laser cavity is designed for generating psec pulses, it supports a large number of modes with frequencies inside a ps^{-1}-wide window, so we expect power fluctuations at the ps time scale. Power fluctuations cause fluctuations in the polariton density and the interaction energy is modulated accordingly. This is the main decoherence mechanism [15]. Indeed, the coherence time of the polariton condensate measured with a Michelson interferometer was $\tau_{\text{coh}} < 5$ ps in that case. In the present experiment, the laser cavity is designed for single-mode operation and a double etalon is placed inside it to suppress all but one mode. The coherence time of the lowest observed polariton mode is $\tau_{\text{coh}} > 26$ ps as evidenced from the resolution-limited linewidth in Fig. 2(b). Measurement with the Michelson interferometer gives the result $\tau_{\text{coh}} \sim 20$ ps, but the real coherence time is expected to be longer, as in this measurement we could not fully suppress the higher modes. This is consistent with the results reported in [16] on a different sample.

We see that pumping with such a laser source creates the appropriate conditions for a steady-state condensate with long coherence time. This is why only the eigenmodes of the gain-induced trap are visible above threshold. On the other hand, when the laser has power fluctuations on short time scale, it introduces an energy uncertainty as explained above. In this case, polaritons condense into a mixed state composed of different modes closely spaced in energy. In particular, phase fluctuations are prominent [12]. The situation is more complicated in highly disordered samples [17], in which case the disorder potential plays a big role in determining in which states polaritons condense.

The nonthermal population distribution among the different modes is due to the nonequilibrium character of polariton condensation and is determined by the pumping and loss rate of every state. In particular, when we change the beam profile from a Π shape to an M shape, so that the pumping density is higher far from the center, the lowest modes are suppressed. The Heisenberg-limited NF and FF distributions of the lowest mode confirm that this state is highly coherent, without substantial phase fluctuations that would introduce energy uncertainty. The interference patterns observed in the FF distributions of the higher modes confirms the coherent character of these states, as well.

We employ a one-dimensional theoretical model similar to the one used in [17]. It consists of two coupled equations, the open dissipative Gross-Pitaevskii equation for the condensate order parameter $\psi(x, t)$ and the rate equation for the reservoir population $n_R(x, t)$

$$i\hbar \frac{\partial \psi(x,t)}{\partial t} = \left\{ -\frac{\hbar^2 \nabla^2}{2m^*} + V_{\text{ext}}(x) - \frac{i\hbar}{2}[\gamma_C - R n_R(x,t)] + g_C |\psi(x,t)|^2 + g_R n_R(x,t) \right\} \psi(x,t), \tag{2}$$

$$\frac{\partial n_R(x,t)}{\partial t} = P_{\text{las}}(x,t) - \gamma_R n_R(x,t) - R n_R(x,t) |\psi(x,t)|^2. \tag{3}$$

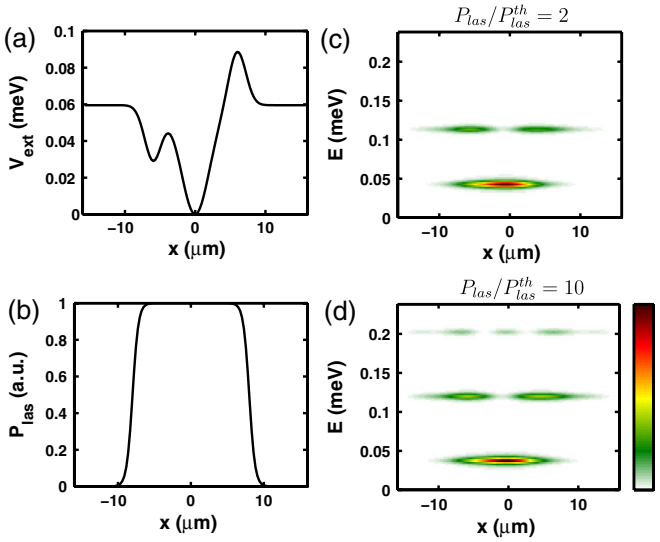

FIG. 5 (color online). Typical results of our theoretical model. (a) We considered the disorder potential $V_{\text{ext}}(x)$ and (b) the laser pumping rate profile $P_{\text{las}}(x)$. (c–d) Real space spectra for different pumping powers, 2 and 10 times, respectively, above threshold. Only the lowest mode is confined by the disorder potential.

$V_{\text{ext}}(x)$ is the external disorder potential and γ_C is the condensate decay rate. For the stimulated scattering rate from the reservoir to the condensate $R \times n_R(x, t)$, we use a linear dependence on the reservoir population. g_C and g_R are the condensate-condensate and condensate-reservoir interaction constants. The reservoir density $n_R(x, t)$ is controlled by the laser pumping rate $P_{\text{las}}(x, t)$ and the reservoir decay rate γ_R. In the time-dependent simulation, $\psi(x, t)$ is a superposition of terms oscillating at different frequencies, which correspond to different modes.

For our simulations, we set the interaction parameters g_C and g_R equal to zero, since when they are small enough they do not influence appreciably the dynamics, but mostly only the energies of the different modes in the steady state. In this case, the stimulated scattering constant R is irrelevant, as a change in its magnitude can be absorbed by the reservoir population $n_R(x, t)$ and the condensate order parameter $\psi(x, t)$ and results in the same equations with a renormalized pumping rate P_{las}. So, we can set R constant and vary only P_{las}. The threshold for condensation $P_{\text{las}}^{\text{th}}$ can be calculated numerically, since below $P_{\text{las}}^{\text{th}}$ the solution $\psi(x, t) = 0$ is stable. The other parameters we used are $m^* = 6 \times 10^{-5} m_e$, $\gamma_C = (3\ \text{ps})^{-1}$, $\gamma_R = (300\ \text{ps})^{-1}$.

Our sample disorder potential is weak [12], so the profile of Fig. 5(a) is a reasonable choice. The results depend on the choice of this potential, but there is no qualitative change as long as it has a local minimum and it is not perfectly symmetric. We also used a top-hat pumping profile with radius of 8 μm [Fig. 5(b)]. Figures 5(c) and 5(d) show the steady-state real space spectra calculated under two different pumping powers above threshold. Excited states not confined by the disorder potential spontaneously appear inside the area pumped by the laser, in qualitative agreement with our experimental results. A detailed comparison with the experiment requires a more complete calculation in a two-dimensional grid, and is beyond the scope of the paper.

We have presented evidence for an inherent effective trapping mechanism of exciton polaritons, which is due to the finite size of the excitation spot along with the short lifetime. Under excitation with an intensity-stabilized laser, several quantized modes of the effective trap spontaneously appear, whose kinetic energies are higher than the disorder potential fluctuations. We observed this quantized mode structure both in real and in momentum space spectra and showed that the real and momentum space distributions of the lowest mode are Heisenberg limited. A one-dimensional model based on the open dissipative Gross-Pitaevskii equation with loss and gain qualitatively reproduces our experimental findings. This trapping mechanism should be present to all samples studied so far.

This work was supported by Navy/SPAWAR Grant No. N66001-09-1-2024, MEXT, and by special coordination funds for promoting science and technology.

*roumpos@stanford.edu

[1] P. C. Hohenberg, Phys. Rev. **158**, 383 (1967).
[2] N. D. Mermin and H. Wagner, Phys. Rev. Lett. **17**, 1133 (1966).
[3] D. Petrov, D. Gangardt, and G. Shlyapnikov, J. Phys. IV (France) **116**, 5 (2004).
[4] C. Weisbuch, M. Nishioka, A. Ishikawa, and Y. Arakawa, Phys. Rev. Lett. **69**, 3314 (1992).
[5] H. Deng *et al.*, Science **298**, 199 (2002).
[6] J. Kasprzak *et al.*, Nature (London) **443**, 409 (2006).
[7] D. Sanvitto *et al.*, Phys. Rev. B **80**, 045301 (2009).
[8] R. Balili *et al.*, Science **316**, 1007 (2007).
[9] D. Bajoni *et al.*, Phys. Rev. Lett. **100**, 047401 (2008).
[10] C. W. Lai *et al.*, Nature (London) **450**, 529 (2007).
[11] G. Roumpos *et al.*, Phys. Rev. B **79**, 195310 (2009).
[12] G. Roumpos *et al.* (to be published).
[13] H. Deng *et al.*, Phys. Rev. Lett. **97**, 146402 (2006).
[14] E. Kapon, *Semiconductor Lasers II* (Academic Press, San Diego, 1999).
[15] D. M. Whittaker and P. R. Eastham, Europhys. Lett. **87**, 27002 (2009).
[16] A. P. D. Love *et al.*, Phys. Rev. Lett. **101**, 067404 (2008).
[17] D. N. Krizhanovskii *et al.*, Phys. Rev. B **80**, 045317 (2009).